Biomass Conversion and Biorefinery (2023) 13:7633–7642
https://doi.org/10.1007/s13399-021-01534-6

ORIGINAL ARTICLE

Cadmium removal by composite copper oxide/ceria adsorbent from synthetic wastewater

Dan Bahadur Pal[1] · Rangabhashiyam Selvasembian[2] · Pardeep Singh[3]

Received: 23 February 2021 / Revised: 19 April 2021 / Accepted: 21 April 2021 / Published online: 19 May 2021

Abstract

Composite copper–ceria-based adsorbent prepared by different sol–gel and co-precipitation methods and their performances were examined for cadmium removal from aqueous solution. Cadmium as a pollutant in drinking water is a severe problem that has negative health effects on humans. In the present study, the prepared adsorbents were characterized using a particle size analyzer, BET surface area, X-ray diffraction (XRD), Fourier transform infrared spectroscopy (FTIR), transmission electron microscopy (TEM), and X-ray photoelectron spectroscopy (XPS) analysis. TEM analysis revealed the presence of approximately hexagonal-shaped copper oxide ceria with size ranging from 15 to 20 nm and having an average size distribution of 15.45 nm for sol–gel and 16.79 nm for co-precipitation prepared adsorbents. Synthesized adsorbents obtained using the sol–gel method showed better cadmium removal than those obtained using co-precipitation methods. Adsorption data of adsorption isotherm and kinetic models were analyzed. Cadmium's adsorption was more rapid in the sol–gel copper oxide ceria adsorbent compared to the co-precipitation copper oxide ceria adsorbent. Equilibrium was attained quickly because of the higher surface area of CuO/CeO_2 prepared by the sol–gel method. The equilibrium adsorption capability of sol–gel copper oxide ceria was more than 93%, while the co-precipitation copper oxide ceria's equilibrium adsorption capability was approximately 89%. The prepared copper–ceria composite adsorbents showed good performance toward cadmium removal from aqueous solutions.

Keywords Adsorption · Cadmium removal · Copper oxide · Cerium oxide · Co-precipitation · sol–gel method

1 Introduction

Manufacturing activities from different industrial sectors produce heavy metals and consequently pollute water bodies. Remediation of water pollutants is essential because freshwater availability is a significantly increasing problem. Toxic heavy metals from different anthropogenic sources directly/indirectly affect the biota and humans [2, 21, 49]. Cadmium (Cd) occurrence in water effluents is sourced from industries such as electroplating, smelting, paint pigments, batteries, fertilizers, mining, and alloy [26]. The occurrence of Cd at higher concentrations in water bodies leads to human consumption that affects vital organs such as the liver, lungs, and kidneys [27]. As per the WHO guidelines, the maximum permissible limit concentration of Cd in drinking water is 1 μg/L. The separation of these harmful metal ions from industrial effluent is an indispensable task to reduce the ecological impacts of Cd ions and comply with the pollution rules and legislation [6]. Many scientists are currently paying attention to water decontamination and desalination methods to conserve water resources worldwide [14, 46, 47, 50, 54, 23].

There are numerous techniques used for removal of Cd from contaminated water such as precipitation [1, 9], ion-exchange [29], membrane separation [34], electro-coagulation [57], photo-catalysis [45], and compared to conventional methods, presented with some drawbacks in the treatment, including inefficient removal, higher operational cost, high power requirements, production of toxic sludge, etc. [8, 24]. Adsorption is considered a suitable method for

✉ Pardeep Singh
psingh.rs.apc@itbhu.ac.in

[1] Department of Chemical Engineering, Birla Institute of Technology, Mesra, Ranchi, Jharkhand 835215, India

[2] Department of Biotechnology, School of Chemical and Biotechnology, SASTRA Deemed University, Thanjavur 613401, India

[3] School of Environmental Studies, PGDAV College of University, New Delhi 110048, India

the remediation of Cd containing effluent with the merits of strong affinity, economical, simple design, effective at low metal concentration, and higher adsorption capacity [10].

The adsorption technique has drawn enormous benefits in efficiency and suitability because of the distribution of different precursors for adsorbent preparations, lower cost, reusable, and easy modifications [5, 46, 47]. Cadmium's removal using the adsorption technique has been reported with adsorbents of customized fibers of activated alumina, Fe oxide, resin, metal oxides, etc. [47, 59]. Furthermore, copper-based adsorbent synthesized from metal oxides or hydroxides showed high surface areas [17]. Recently, copper–ceria-based nanocomposites have received significant attention because of the consistent, stable capability of the functional groups and selectivity [46, 47, 53].

The present research deals with the composite copper–ceria adsorbent prepared by sol–gel and co-precipitation methods. The adsorbents were assessed for their ability to remove Cd from an aqueous solution. Characterization of the prepared adsorbents was carried out using a particle size analyzer, BET surface area, X-ray diffraction (XRD), Fourier transform infrared spectroscopy (FTIR), transmission electron microscopy (TEM), and X-ray photoelectron spectroscopy (XPS) analysis. The adsorption process experimental data were fitted to the two-parameter isotherm model, and the contact time experimental data were analyzed using the adsorption kinetic models.

2 Material and methods

2.1 Chemicals

Chemical cerium nitrate hexahydrate copper nitrate trihydrates, citric acid, acetic acid, ethyl alcohol, NaOH (Merck at purity ~98.9%) were used without further purifications. A standard Cd solution of 1000 μg/ml (Accu Standard) was prepared to make different concentrations of Cd solutions using deionized water.

2.2 Preparation of adsorbent by sol–gel (U1) and co-precipitation (U2) methods

Copper–cerium oxide was prepared following a modified sol–gel method (U_1) reported in the literature [18], in which citric acid (CA) was used as a complexing agent. First, cerium nitrate hexahydrate and copper nitrate trihydrate, mixed in proportions based on the composition, were dissolved in deionized water to form a 0.1 M solution of whole metal ions [43]. Copper–cerium oxide was prepared by the co-precipitation method (U2). Cerium nitrate, copper nitrate, and urea were dissolved in 50 ml of deionized water to get a transparent solution [18]. The initial urea–nitrate molar ratio was taken into account to measure the urea–nitrate stoichiometric molar ratio [43]. The precipitates usually have pH values in the range of 4.0 to 8.0 at ambient temperature.

2.3 Characterization

BET specific surface area measurements of adsorbents were determined using a Micromeritics ASAP 2020 analyzer. Particle size analysis of the adsorbents was determined using a laser diffraction (Helium–Neon Laser, 5 Mill) based particle size analyzer (ANKERSMID, CIS-50, USA). Fourier transform infrared spectroscopy (FTIR) of the synthesized adsorbents was recorded in the range of 400 to 4000 cm^{-1} on a Shimadzu 8400. X-ray measurement of the adsorbents was carried out using a Rigaku Ultima IV X-ray diffractometer (Germany). X-ray photoelectron spectroscopy (XPS) was used to monitor the component's surface concentrations and chemical states and was performed using an Amicus spectrometer. Transmission electron microscopy (TEM) used a model Tecnai G2 20 TWIN, FEI Company of USA.

2.4 Adsorption of Cd

The adsorption on the Cd was studied via varying primary Cd concentration (10 to 50 μg/ml) through 0.71 g/100 ml of CuO/CeO_2 adsorbent and a complete solution amount of 100 ml in a 250 ml container at pH 6.6 and stirring speed 120 rpm. Aliquots (0.5 ml) were removed at regular intervals, and the concentration of Cd was calculated using an atomic absorption spectroscopy (AAS) analyzer (Perkin Elmer, Analyst 800).

3 Results and discussion

3.1 BET surface area and particle size analysis

The standard technique for evaluating the BET surface area is based on the physical adsorption on the concrete surface. The results are 70 m^2/g for the sol–gel preparation method and 60 m^2/g for the co-precipitation preparation method, as shown in Table 1. The copper–ceria adsorbent prepared using the sol–gel method has a larger surface area than that made using the co-precipitation methods. The properties of the copper–ceria-based adsorbent prepared using the sol–gel method lead to better Cd removal than the adsorbent made using the co-precipitation method. While particle size decreases, the experimental scattering angle increases logarithmically. Scattering intensity is also dependent on particle size, diminishing with particle volume [43]. Consequently, large particles scatter light at narrow angles with high

Table 1 Characteristics of the Cu–Ce composite adsorbent

Adsorbent	Components	S_{BET} (m^2/g)	Pore volume (cm^3/g)	Pore size (A^O)	Mean particle size (μm)
U1	Cu–Ce	70	–	–	0.90
U2	Cu–Ce	60	0.0957	54.350	1.08

intensity, and small particles scatter at wider angles but with lower intensity.

3.2 FTIR analysis

The FTIR spectra of the CuO/CeO_2 adsorbent are shown in Fig. 1. The broad bands (3700 to 3000 cm^{-1}) for cerium oxide represent the stretch vibration of the hydroxyl group in chemisorbed water [40, 42, 46]. The significant peaks between 900 and 1629 cm^{-1} after calcination at 500 °C can be seen in the case of cerium oxide, indicating some remaining organic constituents available in the copper–cerium oxide adsorbent. These special functional properties of the copper–ceria-based adsorbent lead to better Cd removal from wastewater. The absorption band's essential improvements (499–1059 cm^{-1}) show cerium oxide formation [55]. The significant peaks of Cd adsorbed by the copper–cerium oxide adsorbent are at wavenumber 3437 cm^{-1} (O–H strong), 2927 cm^{-1} (C–H medium to strong), 1624 cm^{-1} (C=C weak to medium), 1114 cm^{-1} (polysacrides), 1049 cm^{-1} (C–O bond), 975 cm^{-1}, and 470 cm^{-1} (halogens group). After the adsorption of Cd ions, some peaks and shifting of peaks also take place during the adsorption. Other researchers also reported analogous peaks of Cu particles at 3442, 1631, 1019, and 519 cm^{-1} subsequent to chemical groups such as hydroxyl, ether, Cu–O, and other groups, correspondingly [22].

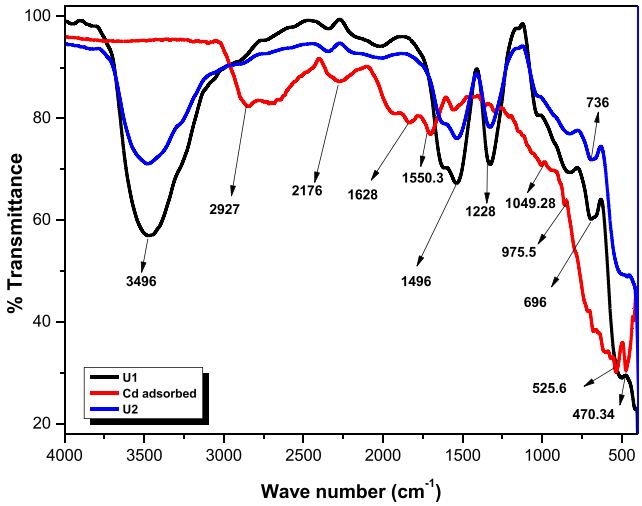

Fig. 1 FTIR of Cu–Ce oxide using U_1 and U_2, respectively, and Cd ions adsorbed on adsorbent

3.3 XRD analysis

The XRD spectra have been compared with the JCPDS files. The XRD spectra of the CuO/CeO_2 composite powder are presented in Fig. 2. The major intense reflections of cerium oxide at a 2θ value of 28.56° and (h, k, l) values (1, 1, 1) are evidently visible, and generally intense reflections of copper oxide are present at a 2θ value of 47.56° and (h, k, l) values (2, 0, 2) are visible [40, 42, 47]. Because of these special properties, the copper–ceria-based adsorbent leads to better Cd removal from aqueous solution. The micrographs exhibit distinctive peaks (111) of a fluorite-like cubic structure and active surfaces in the adsorbent [56].

3.4 XPS analysis

Figure 3 shows the XPS spectra of cerium $3d^{5/2}$ in composite copper–ceria adsorbent: the different methods are coded as sol–gel (U_1) and co-precipitation (U_2). The high-resolution O 1s spectra of cerium oxide material were deconvoluted into three peaks: two oxygen species on the surface zone [33] oxygen moieties jump with Ce(III) and Ce(IV) [40, 42]. The cerium(III) ions composition may be immediate to the oxygen opening on the ceria surface and influence ceria movement such as catalyzing ozonation of aniline, which is straight depending on the increase of cerium(III) species on cerium oxide surfaces [39].

Figure 4 shows the XPS spectra of copper $2p^{3/2}$ in CuO/CeO_2 composite: (a) U_1, (b) U_2, and binding energies of adsorbents prepared. The continuation of a strong metal-support contact between copper and cerium oxide can adapt the

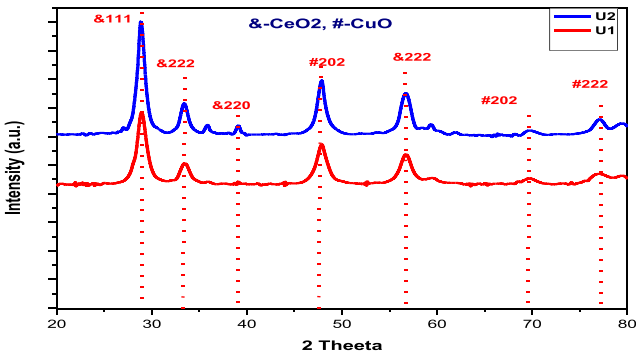

Fig. 2 XRD spectra of the composite Cu/CeO_2 prepared by U_1 and U_2, respectively

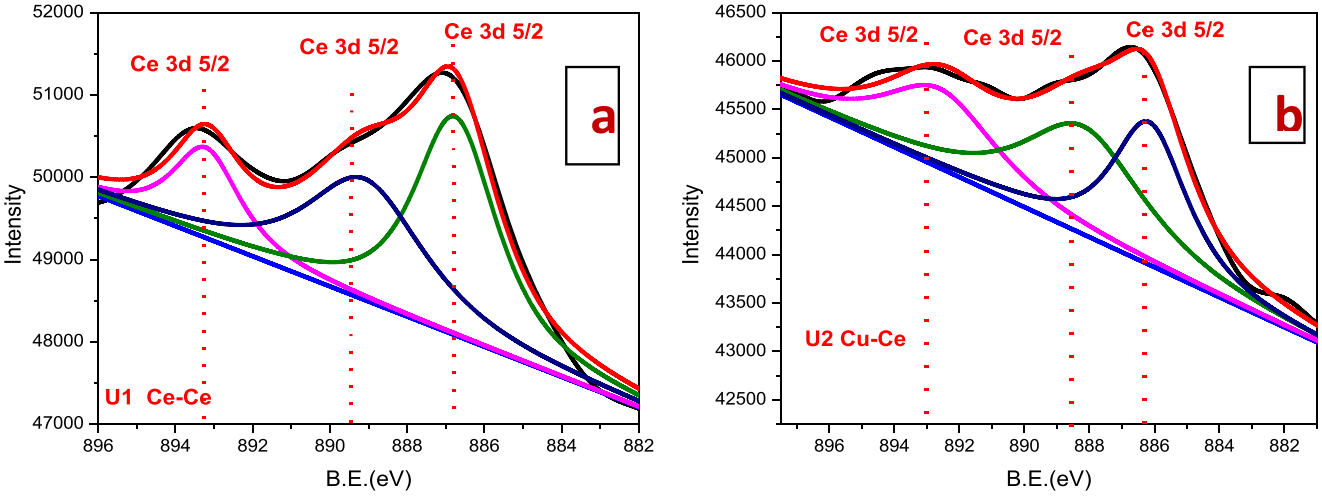

Fig. 3 XPS analysis of Ce $3d^{5/2}$ in Cu/CeO_2 composite: U_1 (**a**) and U_2 (**b**)

structural properties of copper, which could recover this system's catalytic performance [51]. The copper was commenced into cerium oxide, and cerium(III) ions of copper–cerium calcined at the same condition were not completely oxidized to cerium(IV) ions, representing that copper loading leads to the preservation of more cerium(III) ions [32].

3.5 TEM analysis

The TEM analysis showed the crystalline size of the CuO/CeO_2 adsorbent. The typical TEM images of the CuO/CeO_2 adsorbent are shown in Figs. 5 and 6. The TEM images show the different preparation methods, i.e., sol–gel and co-precipitation, with an abundance of roughly hexagonal-shaped CuO/CeO_2 with dimensions ranging from 15 to 20 nm. A size allocation histogram of CuO/CeO_2 corresponding to different TEM images showed that the highest CuO/CeO_2 was in the range of 5 nm to 28 nm and having an average size distribution of 15.5 nm for sol–gel and 16.75 nm for co-precipitation (Figs. 5a and 6a). Selected area electron diffraction (SAED) spectra of CuO/CeO_2 colloid are shown in Figs. 5b and 6b. The typical SAED pattern with bright circular rings revealed that the synthesized CuO/CeO_2 was crystalline.

3.6 Kinetics study of Cd removal

The adsorption of Cd on the CuO/CeO_2 at various initial concentrations was studied. Figure 7 shows the varying of adsorbed Cd depending on the reaction time. Cadmium adsorption was more rapid in the sol–gel CuO/CeO_2 adsorbent compared to the co-precipitation CuO/CeO_2 adsorbent. It required less time to attain equilibrium because of the larger surface area of CuO/CeO_2 prepared using the sol–gel method. More than 93% of the equilibrium adsorption capability was reached within 1 h for the sol–gel CuO/CeO_2 adsorbent.

In comparison, it took approximately 60 min to attain 89% of the co-precipitation copper oxide ceria's equilibrium adsorption capability. Because of the large surface area of CuO/CeO2 and its dispersed nature, Cd's removal percentage was quite high. Other researchers [36] also investigated the Cd

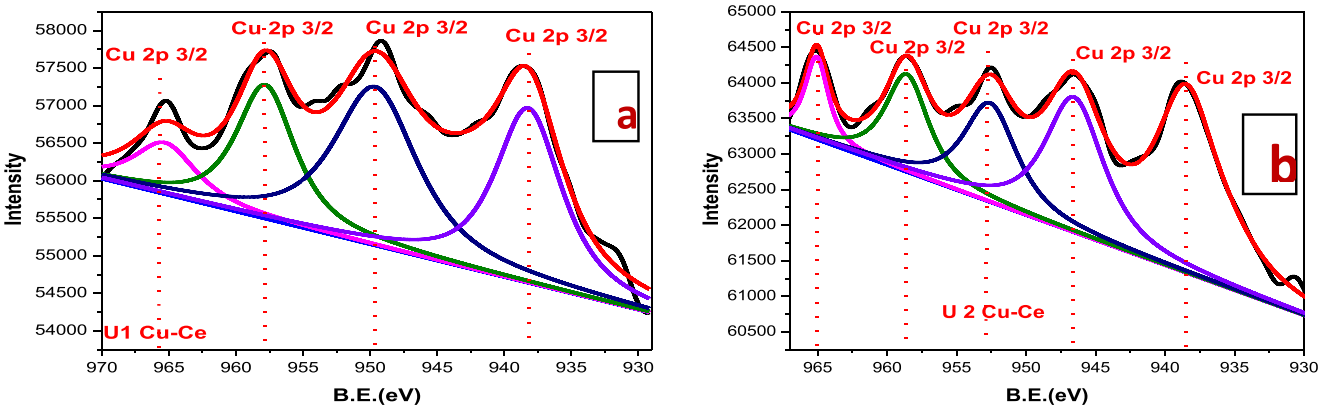

Fig. 4 XPS analysis of Cu $2p^{3/2}$ in Cu/CeO_2 composite: U_1 (**a**) and U_2 (**b**)

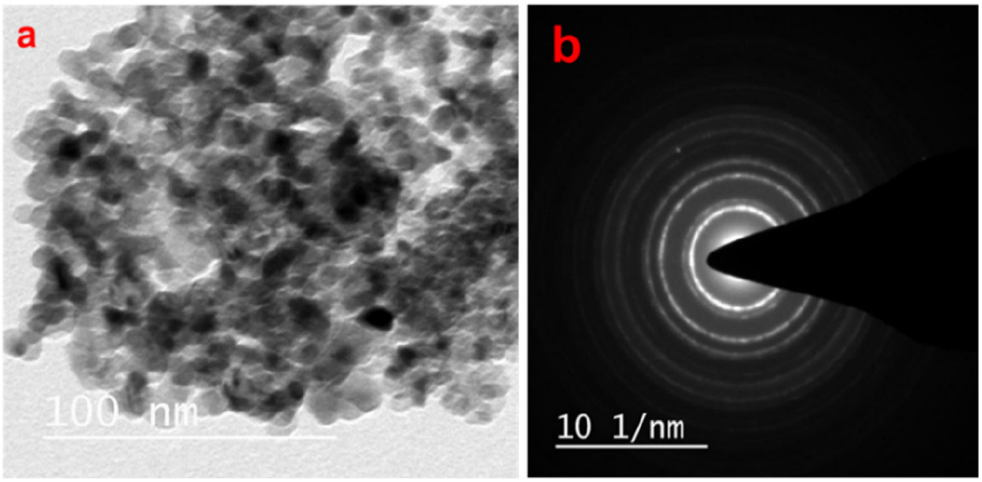

Fig. 5 (**a**) and (**b**) TEM analysis of composite CuO/CeO_2 prepared using the sol–gel method

removal from chicken eggshell adsorbent for theoretical Cd removal effectiveness based on the produced model of 75.3% less removal within a 75 min contact time, which also required more time than the current study. The occurrence of the unique chemical groups such as hydroxyl, carbonyl, and others explains an elevated removal [36]. It contains dynamic binding sites that enhanced adsorptive components in heavy metals such as Cd. This means removal efficiency greater than 93% was achieved, which is more than the values (75%) found in a previous study. The time taken for removal was approximately 90 min, and the present study's maximum time was 60 min [44, 48].

The calculation of kinetics is essential for the design of adsorption systems and reaction rate-controlling step, to ensure a chemical reaction occurs. The adsorption process's nature depends on the adsorbent's physicochemical characteristic and system conditions such as temperature [37]. The amount of metals adsorbed, qt, at time t was calculated using the following equation:

$$q_t = \frac{(C_0 - C_e)\,V}{W} \tag{1}$$

where q_t is adsorption capacity at time t (mg/g), C_o is the initial metal ion concentration (mg/ L), C_e is the metal ion concentration at equilibrium (mg/ L), V is the volume of solution (L), W is the weight of the bio-adsorbent (g), and q_{cd} ion is the adsorption capacity at equilibrium (mg/ g).

Pseudo-first-order and pseudo-second-order models were used to fit the adsorption data, and four kinetic fitting curves were obtained. The pseudo-first-order equation of Lagrange is generally expressed as follows [16]:

$$\log(q_e - q_t) = \log q_e + \frac{k_1}{2.303}t \tag{2}$$

The pseudo-second-order rate expression is based on the solid phases' sorption capacity (include citation), which has been applied for analyzing kinetics rate of chemisorption. It is given by:

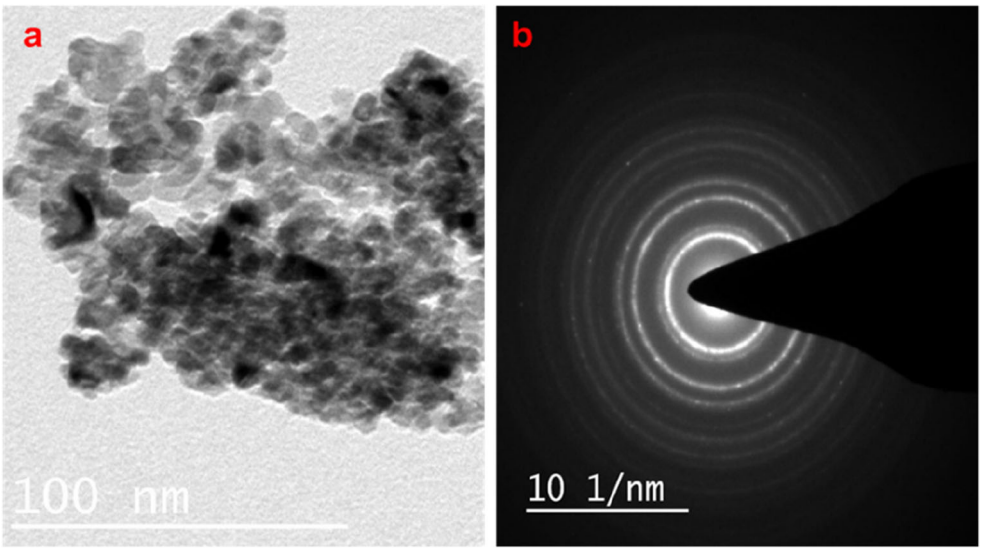

Fig. 6 (**a**) and (**b**) TEM analysis of composite CuO/CeO_2 prepared using the co-precipitation method

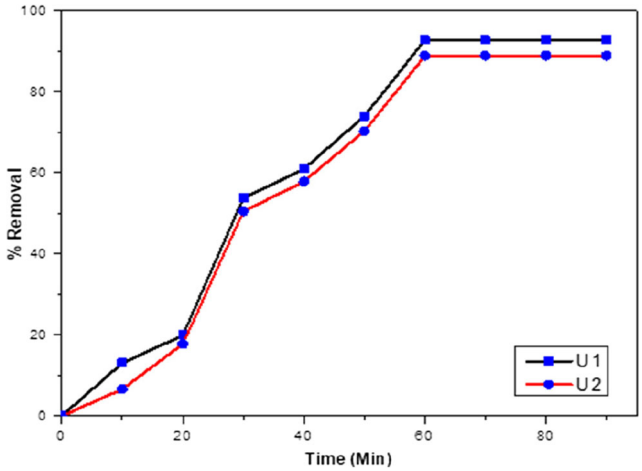

Fig. 7 Kinetics of Cd removal by the composite Cu/CeO_2 at initial concentrations 40 ppm, for adsorbent dose 3.35 g/500 ml, pH 6.5 ± 0.5, temperature 32 °C

$$\frac{t}{q_t} = \frac{1}{q_e^2\, k_2} + \frac{t}{q_e} \tag{3}$$

After again computing the variation of Cd adsorption kinetics on the CuO/CeO_2, the pseudo-first-order and pseudo-second-order kinetic data were utilized to understand the adsorption kinetics (Figs. 8 and 9). The kinetics analysis was achieved by fitting the adsorption data to the kinetic models and the results are shown in Table 2. As per the regression analysis results (R^2), the experimental values fit the pseudo-first-order data superior to the pseudo-second-order data for Cd [40–42].

The nonlinear kinetic models described in Table 2 are shown in Fig. 8a, b, and computed coefficients are tabulated in Table 2. The constants of U_1 and U_2 were k_1 0.074 per min and 0.0335 per min, respectively, for the first-order, and k_2 were 0.00061 and 0.0129 (g/mg min), respectively, for the second-order kinetic model, and R^2 values of U_1 and U_2 were 0.97 and 0.98 for the first-order and 0.67 and 0.45 for the second-order model, respectively. The calculated equilibrium capacities are 7.43 mg/g and 3.217 mg/g for CuO/CeO_2 sol–gel and CuO/CeO_2 co-precipitation methods, respectively, for the pseudo-first-order model, showing that the Cd adsorption to CuO/CeO2 sol–gel fitted to this model. Other studies, as shown in Table 2, used white sandstone as the base material for a nano-silica generation [28]. Meanwhile, the values of sol–gel CuO/CeO_2 k_2 were higher than those of co-precipitation CuO/CeO_2 under similar conditions. Cadmium concentration reduction was better by the previous compared to the later one. The adsorption capability of composite CuO/CeO_2 and several other adsorbents for Cd metal ions are collected from the literature [25, 60]. Cadmium composition in normal polluted waters is generally less. Therefore, it is more logical to estimate the adsorption performance of Cd at a small equilibrium Cd composition. With the lower equilibrium Cd composition, the adsorption value might better suit the French model. At the equilibrium Cd composition of 0.01 mg/L as the Cd standard for consumption water, Cd's adsorption capability was approximately 6.86 mg/g for Cd [41, 58]. From this data, it is reasonably clear that the adsorption capacity of CuO/CeO_2 is relatively high compared to other adsorbent resources [36].

Langmuir and Freundlich models are used to fit the adsorption isotherm, which is represented below:

The Langmuir isotherm assumes monolayer adsorption on a uniform surface with a finite number of adsorption sites. This model is presented by the following equation [30, 31].

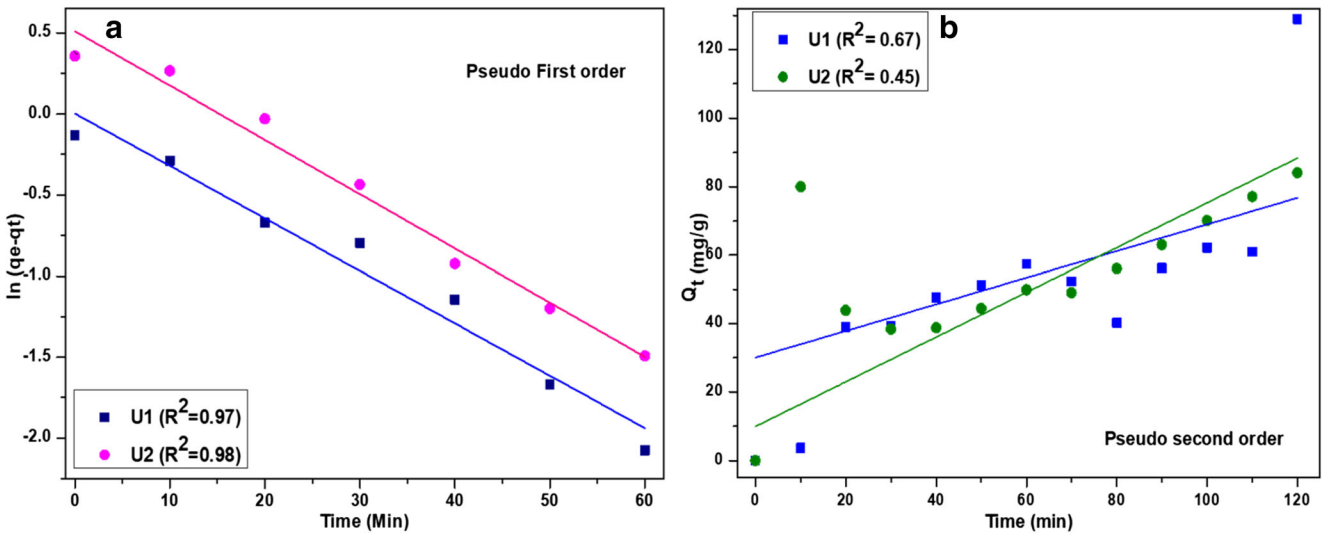

Fig. 8 Adsorption kinetics of Cd by Cu/CeO_2 adsorbent for pseudo-first-order and -second-order models

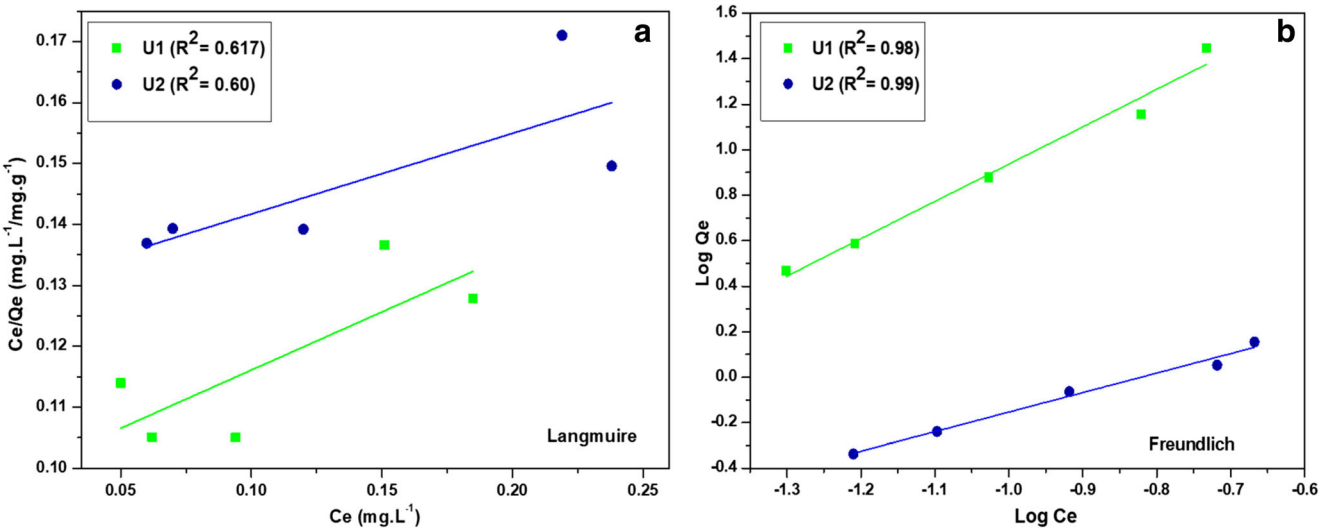

Fig. 9 Adsorption isotherm of Cd by CuO/CeO_2 for Langmuir (**a**) and Freundlich (**b**) models

Table 2 Kinetics parameters for Cd(II) adsorption using U1 and U2

Treatment	Initial concentration	Pseudo-1st-order kinetics $\ln(Qe-Qt)=\ln Qe-k1t$			Pseudo-2nd-order kinetics $\frac{t}{Qt}=\frac{1}{k2Qe2}+\frac{t}{Qe}$		
		k_1 min^{-1}	Qe (mg g^{-1})	R^2	K_2 (g/mg min)	Qe (mg g^{-1})	R^2
Present study [U1]	40 mg/L	0.074	7.43	0.97	0.00061	6.71	0.67
Present study [U2]	40 mg/L	0.0335	3.217	0.98	0.0129	2.574	0.45

The linear form of the Langmuir isotherm is described as:

$$\frac{C_e}{q_e}=\frac{1}{q_m b_0}+\frac{tC_e}{q_m} \quad (4)$$

Values of Langmuir parameters q_m and b_0 are calculated from the slope and intercept of the linear plot C_e/q_e versus C_e.

The purpose of the Freundlich equation also suggests that sorption energy exponentially decreases upon the completion of the sorption centers of the adsorbent [20].

Freundlich equilibrium constants could be determined from the linear plot of ln qe and ln Ce according to the following equation:

$$\ln q_e=\ln K_f+\frac{1}{n}\ln C_e \quad (5)$$

The Freundlich isotherm is widely applied in heterogeneous systems, especially organic compounds or highly interactive species on activated carbon and molecular sieves [19].

From Table 3, it is proposed that Freundlich more adequately describes the data than other studied models. The finding suggests the surface of CuO/CeO_2 sol–gel and CuO/CeO_2 co-precipitation methods for Cd adsorption. The higher attraction capacity (6.86 mg/g) for Cd removal was higher than the CuO/CeO_2 sol–gel preparation method. Table 3 compares the maximum attraction of Cd ions using CuO/CeO_2 sol–gel and CuO/CeO_2 co-precipitation methods with other used adsorbents in the literature and shows that both adsorbents are effective in the removal of the objective purity. Also, the R^2 value of the Freundlich isotherm model for Cd ion adsorption using CuO/CeO_2 sol–gel and CuO/CeO_2 co-precipitation methods were 0.98 and 0.99, respectively, indicating that the

Table 3 Comparative equilibrium isotherm parameters of Cd adsorption on the U1 and U2

Isotherm model	Parameters	U1	U2
Langmuir model	b_o	0.197	0.1447
	q_m(mg/g)	6.86	1.31
	R^2	0.617	0.60
Freundlich model	K_f (mg/g)	4.465	2.237
	n	0.389	0.869
	R^2	0.98	0.99

Table 4 Comparison of different adsorbents used for cadmium removal from water

Adsorbent	$C_{initial}$ (mg/L)	$q_{e,\ max}$ (mg/g)	$q_{e,0.01}$ (mg/g)	pH	Reference
TiO_2: granular	80	41.4	<3.0	7.0	[7]
CeO_2-Si nanocomposite	50	22.820	<4.01	1-8	[47]
Polyaluminum granulate	280	14.85	<0.07	7.5	[35]
White sandstone	20	6.824	<7.01	2-10	[46]
Fe oxide coated sponge	5	4.05	<0.5	6.5–7.3	[38]
Nano-silica	20	6.873	<7.01	2-10	[46]
U1	40	7.43	< 0.54	4-9	Present study
U2	40	3.217	< 0.50	4-9	Present study

Freundlich isotherm model has fair potential to investigate the equilibrium behavior of Cd ion adsorption by CuO/CeO_2 sol–gel [52].

The assessment of the copper oxide ceria's adsorption capacity among other substances at lower equilibrium Cd composition is shown in Table 4. Figure 10a, b depicts the trend of variation in removal percentage of Cd with various doses and pH. Figure 10b depicts the effect of initial pH on the equilibrium adsorption capacity of biosorbent. It is observed that at pH 6.6, a maximum removal percentage (92.78%) was obtained at approximately 60 min using the copper–ceria prepared by sol–gel, after which it stabilizes. Thus, pH 6.6 is found to be the optimum pH at which maximum Cd removal takes place. At a very low pH, the adsorption decreases as the hydrogen ion itself competes with the Cd ions for adsorption [4, 13, 15]. As the pH increases, adsorption ability enhances due to an increase in the negative charge on the surface of the adsorbent walls. However, as we go toward alkaline pH, the adsorption again decreases as the metal ions in the solution precipitate out, obstructing the procedure. In general, a range of pH 2–8 is favorable for Cd ion adsorption [3, 11, 12, 15]. Rauf et al. [46] also investigated Cd removal with increasing pH, where the uptake efficiency elevated, and this trend continued until the initial pH of 6. Then with increasing pH, the efficiency reduces due to Cd(II) sequestration. As observed, with increasing initial Cd ion concentration, the adsorption efficiency decreases [46].

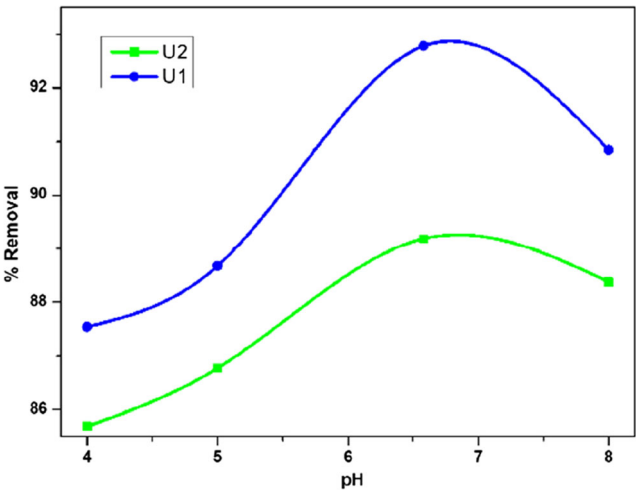

Fig. 10 Cadmium removal (%) at different pH of synthetic contaminated solution with cadmium

4 Conclusion

The copper–ceria adsorbent composites prepared using sol–gel and co-precipitation methods were effective for Cd removal from aqueous solution. Cd adsorption was higher and more rapid in the sol–gel CuO/CeO_2 adsorbent compared to the co-precipitation CuO/CeO_2 adsorbent. Because CuO/CeO_2 prepared using the sol–gel method has higher surface area and small particle size, it required less time to attain equilibrium. The sol–gel CuO/CeO_2 had more than 93% equilibrium adsorption efficiency, while the co-precipitation CuO/CeO_2 had approximately 89% equilibrium adsorption efficiency. TEM showed that the sol–gel and co-precipitation methods made an abundance of approximately hexagonal-shaped CuO/CeO_2 with size ranging from 15.0 to 20.0 nm and having an average size distribution of 15.45 nm for sol–gel and 16.79 nm for co-precipitation. The Freundlich kinetic model well-described the adsorption process of Cd using adsorbent based on the CuO/CeO_2 sol–gel method. The adsorption kinetic models of Cd removal were better explained using the pseudo-first-order model.

Acknowledgements The authors acknowledge Birla Institute of Technology, Mesra, Ranchi, JH and Indian Institute of Technology (BHU), Varanasi for characterization and raw materials, respectively, and NPIU (TEQIP-III), Delhi, Govt. of India for the financial support.

Author's contributions Dr. Dan Bahadur Pal conducted all experiments, processed experimental data, and prepared the manuscript's first draft. Dr.

Pardeep Singh and Dr. Rangabhashiyam Selvasembian helped in the work's progress, provided useful suggestions, and finalized the experimental protocol, critically analyzing the results.

Funding The funding agencies (NPIU/AICTE New Delhi, India) have been duly acknowledged and also all Co-PIs of the project.

Declarations

Ethical No data or figures have been fabricated or manipulated.

Consent to publish All the co-authors have seen the final manuscript and agreed with the submission to the journal.

Competing interests The authors have no conflicts of interest to declare that are relevant to the content of this article.

References

1. Abid BA, Brboot MM, Al-ShuwaikI NM (2011) Removal of heavy metals using chemicals precipitation. Eng Technol J 29:595–612
2. Ahmed DN, Naji LA, Faisal AAH, Ansari NA, Naushad M (2020) Waste foundry sand/MgFe-layered double hydroxides composite material for efficient removal of Congo red dye from aqueous solution. Sci Rep 10:2042
3. Arroub H, Hsissou R, El Harfi A (2019) Adsorption of Zn2+ and Cu2+ ions by activated carbon prepared from dates stones computational approach. Anal Bioanal Electrochem 11(10):1398–1413
4. Arroub H, Hsissou R, Elharfi A (2020) Investigation of modified chitosan as potential polyelectrolyte polymer and eco-friendly for the treatment of galvanization wastewater using novel hybrid process. Results Chem 2:100047
5. Awual MR, Hasan MM, Shahat A (2014) Functionalized novel mesoporous adsorbent for selective lead(II) ions monitoring and removal from wastewater. Sens Actuators B: Chem 203:854–863
6. Bailey SE, Olin TJ, Bricka RM, Adrian DD (1999) A review of potentially low-cost sorbents for heavy metals. Water Res 33(11): 2469–2479
7. Bang S, Patel M (2005) Advanced materials for agriculture, food and environmental safety. Chemosphere 60:389–397
8. Barakat MA (2011) New trends in removing heavy metals from industrial wastewater. Arab J Chem 4:361–377
9. Baskan MB, Pala A (2009) Determination of arsenic removal efficiency by ferric ions using response surface methodology. J Hazard Mater 166:796–801
10. Bunmahotama W, Hung WN, Lin TF (2015) Predicting the adsorption of organic pollutants from water onto activated carbons based on the pore size distribution and molecular connectivity index. Water Res 85:521–531
11. Es-sahbany H, Hsissou R, El Hachimi ML, Allaoui M, Nkhili S, Elyoubi MS (2021a) Investigation of the adsorption of heavy metals (Cu, Co, Ni and Pb) in treatment synthetic wastewater using natural clay as a potential adsorbent (Sale-Morocco). Mater Today Proc. https://doi.org/10.1016/j.matpr.2020.12.1100
12. Es-sahbany H, Hsissou R, El Hachimi ML, Allaoui M, Nkhili S, Elyoubi MS (2021b) Adsorption of heavy metal (Cadmium) in synthetic wastewater by the natural clay as a potential adsorbent (Tangier-Tetouan-Al Hoceima – Morocco region). Mater Today Proc. https://doi.org/10.1016/j.matpr.2020.12.1102
13. Es-Sahbany H, Berradi M, Nkhili S, Hsissou R, Allaoui M, Loutfi M et al (2019) Removal of heavy metals (nickel) contained in wastewater-models by the adsorption technique on natural clay. Mater Today Proc 13:866–875
14. Faisal AAH, Al-Wakel SFA, Assi HA, Naji LA, Naushad M (2020) Waterworks sludge-filter sand permeable reactive barrier for removal of toxic lead ions from contaminated groundwater. J Water Process Eng 33:101112
15. Fan T, Liu Y, Feng B, Zeng G, Yang C, Zhou M, Zhou H, Tan Z, Wang X (2008) Biosorption of cadmium (II), zinc(II) and lead(II) by Penicillium simplicissimum: isotherms, kinetics and thermodynamics. J Hazard Mater 160:655–661
16. Farhan AM, Salem NM, Al-Dujaili AH, Awwad AM (2012) Biosorption of Cr(VI) ions from electroplating wastewater by walnut Shell powder. Am J Environ Eng 2(6):188–195
17. Feng LY, Cao MH, Ma XY, Zhu YS, Hu CW (2012) Super paramagnetic high surface area Fe_3O_4 nanoparticles as adsorbents for arsenic removal. J Hazard Mater 227:484
18. Ferreira AC, Ferraria AM, do Rego AB, Gonçalves AP, Girão AV, Correia R, Gasche TA, Branco JB (2010) Partial oxidation of methane over bimetallic copper–cerium oxide catalysts. J Mol Catal A Chem 320(1-2):47–55
19. Foo KY, Hameed BH (2010) Insights into the modeling of adsorption isotherm systems. Chem Eng J 156(1):2–10
20. Freundlich HMF (1906) Uber die adsorption in losungen. Z Phys Chem 57(A):385–470
21. Gebru KA, Das C (2018) Removal of chromium (VI) ions from aqueous solutions using amine-impregnated TiO2 nanoparticles modified cellulose acetate membranes. Chemosphere 191:673–684
22. Goswami A, Raul PK, Purkait MK (2012) Arsenic adsorption using copper (II) oxide nanoparticles. Chem Eng Res Des 90(9):1387–1396
23. Habiba U, Afifi AM, Salleh A, Ang BC (2017) Chitosan/(polyvinyl alcohol)/zeolite electrospun composite nanofibrous membrane for adsorption of Cr6+, Fe3+ and Ni2+. Journal Hazard Mater 322: 182–194
24. Hariharan A, Harini V, Sandhya S, Rangabhashiyam S (2020) Waste *Musa acuminata* residue as a potential biosorbent for the removal of hexavalent chromium from synthetic wastewater. Biomass Convers Bior. https://doi.org/10.1007/s13399-020-01173-3
25. Heidari A, Younesi H, Mehrabanb Z, Heikkinenc H (2013) Selectiveadsorption of Pb(II), cd(II), and Ni(II) ions from aqueous solution usingchitosan-MAA nanoparticles. Int J Biol Macromol 61:251–263
26. Iqbal M, Edyvean RGJ (2005) Loofa sponge immobilized fungal biosorbent: a robust system for cadmium and other dissolved metal removal from aqueous solution. Chemosphere 61:510–518
27. Jarup L, Åkesson A (2009) Current status of cadmium as an environmental health problem. Toxicol Appl Pharm 238:201–208
28. Karim MR, Aijaz MO, Alharth NH, Alharbi HF, Al-Mubaddel FS, Awual MR (2019) Composite nanofibers membranes of poly(vinyl alcohol)/chitosan for selective lead(II) and cadmium(II) ions removal from wastewater. Ecotoxicol Environ Safety 169:479–486
29. Kumar R, Chawla J (2014) Removal of cadmium ion from water/wastewater by nanometal oxides: a review. Water Qual Expos Health 5:215–226
30. Langmuir I (1918) The adsorption of gases on plane surface of glass, mica and platinum. J Am Chem Soc 40(9):1361–1403
31. Langmuir I (1916) The constitution and fundamental properties of solids and liquids. Part I. Solids. J Am Chem Soc 38(11):2221–2295
32. Lei L, Song L, Chen C, Zhang Y, Zhan Y, Lin X, Zheng Q, Wang H, Ma H, Ding L, Zhu W (2014) Modified precipitation processes and optimized copper content of CuO-CeO_2 catalysts for water gas shift reaction. Int J Hyd Energy 39:19570–19582

33. Li ZJ, Deng SB, Yu G, Huang J, Lim VC (2010) As(V) and as(III) removal from water by a Ce-Ti oxide adsorbent: behavior and mechanism. Chem Eng J 161:106–113
34. Malik AH, Khan ZM, Mahmood Q, Nasreen S, Bhatti ZA (2009) Perspectives of low cost arsenic remediation of drinking water in Pakistan and other countries. J Hazard Mater 168:1–12
35. Mertens J, Rose J, Kagi R, Chaurand P, Plotze M, Wehrli B, Furrer G (2012) Adsorption of arsenic on polyaluminum granulate. Environ Sci Technol 46:7310–7317
36. Mittal A, Teotia M, Soni RK, Mittal J (2016) Applications of egg shell and egg shell membrane as adsorbents: a review. J Mol Liq 223:376–387
37. Nadeem M, Mahmood A, Shahid SA, Shah SS, Khalid AM, McKay G (2006) Sorption of lead from aqueous solution by chemically modified carbon adsorbents. J Hazard Mater 138(3):604–613
38. Nguyen TV, Vigneswaran S, Ngo HH, Kandasamy J (2010) Arsenic removal by iron oxide coated sponge: experimental performance and mathematical models. J Hazard Mater 182:723–729
39. Orge CA, Orfao JJM, Pereira MFR, de Farias AMD, Fraga MA (2012) Ceria and cerium-based mixed oxides as ozonation catalysts. Chem Eng J 200-202:499–505
40. Pal DB, Giri DD, Singh P, Pal S, Mishra PK (2017a) Arsenic removal from synthetic waste water by CuO nano-flakes synthesized by aqueous precipitation method. Desalination Wastewater Treat 62:355–359
41. Pal DB, Lavania R, Srivastava P, Singh P, Madhav S, Mishra PK (2018) Photo-catalytic degradation of methyl tertiary butyl ether from wastewater using CuO/CeO2 composite nanofiber catalyst. J Environ Chem Eng 6:2577–2587
42. Pal DB, Singh P, Mishra PK (2017b) Composite ceria nanofiber with different copper loading using electrospinning method. J Alloys Comp 694:10–16
43. Pal DB, Prasad R (2014) Study of water gas shift reaction. Lambert, Sunnyvale, p 5
44. Poinern GEJ, Brundavanam S, Tripathy SK, Suar M, Fawcett D (2016) Kinetic and adsorption behavior of aqueous cadmium using a 30 nm hydroxyapatite based powder synthesized via a combined ultrasound and microwave based technique. Phys Chem 6:11–22
45. Rahimi S, Ahmadian M, Barati R, Yousefi N, Moussavi SP, Rahimi K et al (2014) Photocatalytic removal of cadmium (II) and lead (II) from simulated wastewater at continuous and batch system. Int J Environ Health Eng 3:90–94
46. Rauf F, Reza M, Seyed JP, Jalali S, Ramavandi B (2020) Application of nano-silica particles generated from offshore white sandstone for cadmium ions elimination from aqueous media. Environ Technol Innov 19:101031
47. Rehab M, Elhassan AA, Mohamed EM (2020) Functionalization of CeO2-SiO2-(CH2)3-cl nanoparticles with sodium alginate for enhanced and effective CdII, PbII, and ZnII ions removal by microwave irradiation and adsorption technique. Environ Nanotechnol Monit Manag 14:100367
48. Said B, M'rabet S, Hsissou R, El Harfi A (2020) Synthesis of new low-cost organic ultrafiltration membrane made from Polysulfone/Polyetherimide blends and its application for soluble azoic dyes removal. J Mater Res Technol 9(3):4763–4772
49. Samal K, Das C, Mohanty K (2016) Development of hybrid membrane process for Pb bearing wastewater treatment. J Water Process Eng 10:30–38
50. Selvakumar A, Rangabhashiyam S (2019) Biosorption of rhodamine B onto novel biosorbents from Kappaphycus alvarezii, Gracilaria salicornia and Gracilaria edulis. Environ Pollut 255(2019):113291
51. Senanayake SD, Rodriguez JA, Stacchiola D (2012) Electronic metal support interactions and the production of hydrogen through the water-gas shift reaction and ethanol steam reforming: fundamental studies with well-defined model catalysts. J Phys Chem C 116:9544–9549
52. Shafiee M, Foroutan R, Fouladi K, Ahmad Louydara M, Ramavandi B, Sahebi S (2019) Application of oak powder/Fe3O4 magnetic composite in toxic metals removal from aqueous solutions. Adv Powder Technol 30:544–554
53. Shahat A, Hassan HMA, Azzazy HME, El-Sharkawy EA, Abdou HM, Awual MR (2018) Novel hierarchical composite adsorbent for selective lead(II) ions capturing from wastewater samples. Chem Eng J 332:377–386
54. Sharma S, Vishal D, Pankaj R, Ahmad HB, Pardeep S, Van-Huy N (2021) Tailoring cadmium sulfide-based photocatalytic nanomaterials for water decontamination: a review. Environ Chem Lett 19:271–306
55. Turkovic A, Dubcek P, Bernstorff S (1999) Grazing-incidence small-angle and wide-angle scattering of synchrotron radiation on nanosized CeO_2 thin films. Mat Sci Eng B Solid-State Mat Adv Tech 58:263–269
56. Van Esch H, Bauters M, Ignatius J, Jansen M, Raynaud M, Hollanders K, Lugtenberg D, Bienvenu T, Jensen LR, Gecz J, Moraine C, Marynen P, Fryns JP, Froyen G (2005) Duplication of the MECP2 region is a frequent cause of severe mental retardation and progressive neurological symptoms in males. Am J Hum Genet 77(3):442–453
57. Vasudevan S, Lakshmi J, Sozhan G (2011) Effects of alternating and direct current in electrocoagulation process on the removal of cadmium from water. J Hazard Mater 192:26–34
58. Wang J, Xu W, Chen L, Huang X, Liu J (2014) Preparation and evaluation of magnetic nanoparticles impregnated chitosan beads for arsenic removal from water. Chem Eng J 251:25–34
59. Xu WH, Wang J, Wang L, Sheng GP, Liu JH, Yu HQ, Huang XJ (2013) Enhanced arsenic removal from water by hierarchically porous CeO_2-ZrO_2 nanospheres: role of surface- and structure-dependent properties. J Hazard Mater 260:498–507
60. Zheng L, Zhu C, Dang Z, Zhang H, Yi X, Liu C (2012) Preparation of cellulose derived from corn stalk and its application for cadmium ion adsorption from aqueous solution. Carbohydr Polym 90:1008–1015